On Similarity Waves in Compacting Media

Fei Dong, Daniel N. Riahi

Department of Theoretical and Applied Mechanics,
University of Illinois at Urbana-Champaign

and

Albert T. Hsui

Department of Geology,
University of Illinois at Urbana-Champaign

Abstract

Compaction generally refers to the relative motion of fluid with respect to the deformable surroundings in a two-phase system. It has many geophysical and engineering applications, including liquefaction, formation of magma chamber, genesis of igneous rocks, foam drainage, and flow in sediments. In this paper, we followed McKenzie's two-phase flow formulation (1984) to study the flow through a porous medium, which is a commonly used model for compaction study. Using the same approach as Barcilon and Lovera (1989), we studied the wave solution with and without melting effect, under the assumption that the ambient porosity is small. Similarity waves were of particular interest here. We discussed the necessary conditions for a specific class of similarity waves to exist, followed by the general behavior of such waves and numerical determination of the solution for several cases. Parametric studies were also carried out to investigate the dependence of the solution on factors such as the melting rate, the density ratio, and the permeability of the solid matrix, etc.

Keywords: Two-phase flow, Compaction, Porous media, Permeability, Porosity, Similarity waves.

Contents

List of Tables

List of Figures

1 Introduction

It has been long observed in the field that large volume of molten rocks in the Earth's interior were either extruded onto the surface or existing in the form of magma chambers beneath the surface. However, laboratory studies for Earth materials under pressure and temperature conditions comparable to those of Earth interior only showed small degree of partial melting. Therefore, the observed large volume of molten rock must either have segregated from the surroundings or have migrated all the way from deep inside the Earth[1]. From this point of view, the information about the relative motion of the magma with respect to the surrounding rocks can be essential in understanding this geophysical problem.

On the other hand, experimental studies in the genesis of igneous rocks showed that an interconnected network can be formed by enormous pores within the partially molten crystalline matrix (see Figure 1) and the melt can therefore flow through the matrix[2]. Such observations have then motivated studies to treat the buoyancy-driven flow of melt

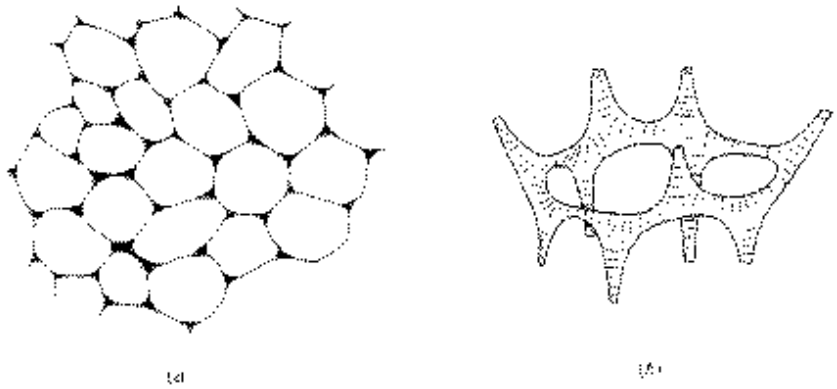

Figure 1: Diagrams of melt distribution: (a) Grains with melt in-between in two-dimensional case. (b) Formation of a three-dimensional interconnected network from the melt. (From Barcilon & Richter[1], reprinted with the permission of Cambridge University Press)

through partially molten rock as the initial process leading to magma segregation in the Earth's interior.

Besides magma segregation, there are many other geophysical applications where a particular fluid flows through a viscously deformable and permeable matrix, including flow of water or oil in sediments. There are also many other engineering applications, such as flow of melt during material processing (melt flow in crystalline matrix), liquefaction

(underground flow of water in soil), and drainage (flow of liquid in bubbles). The common feature of all the applications is the relative motion of a fluid with respect to a deformable surroundings in a two–phase system. In describing such flows, the term "compaction" is commonly used in literature to refer to the ability of the surrounding medium to compact (or deform) such that relative motions between the fluid and the medium are produced.

In this paper we shall start with the general mathematical description of a melt–matrix system in section 2, using the model developed by McKenzie and his coworkers[3, 4]. From section 3 and thereafter, we will be focusing on waves propagating in such a system, particularly those solutions referred to as the similarity waves. The formulation and existence conditions are described in section 3, while the general behavior of such wave solutions is discussed in section 4. Solutions in three different cases are then determined numerically and compared in section 5, followed by a parametric study of the dependence of the solutions on different factors, such as the melting rate, the density ratio, and the permeability of the solid matrix. Finally, concluding remarks are made in the last section.

2 General Formulation

As illustrated in Figure 1, melt appears in the clearance between the grain boundaries in two dimensions, while in three dimensions it forms an interconnected network around the grains. In either case, it is appropriate to apply a continuum description to this system since the grain size is usually very small compared with the characteristic length scale of the flow region. A commonly used approach to model the flow is the two–phase description. Readers are referred to McKenzie[3] and Richter & McKenzie[4] for details about this modeling approach. Without going into all the details, this model treats the solid matrix and the melt as two fluids of constant, but different, density. It assumes that the two fluids interpenetrates each other and the contact surfaces are so convoluted that it is appropriate to define a porosity field $\phi(\vec{x}, t)$, which represents the volume fraction of the melt. The solid matrix is treated as an active porous medium with finite bulk viscosity to capture its compacting ability, and Darcy's Law is employed for convenience to relate the relative velocity field to the pressure gradient. For simplicity, it is further assumed that the permeability K of the matrix, which is a measure of the ability of a flow to traverse the porous region, can be related to the porosity ϕ by a power law

$$K = K_0 \left(\frac{\phi}{\phi_0} \right)^n , \tag{2.1}$$

where the quantities with a superscript "0" are the reference values, and $n = 3$ represents a good estimate based on experimental results with low percentage melting.

At this stage, only the dynamics of the system is considered. In other words, thermodynamic aspects such as heat exchange from the phase change and all other kinds of heat transport are not included in the model. Under this consideration, the governing equations for the two-phase system are given as follows:

$$\frac{\partial \phi}{\partial t} + \nabla \cdot (\phi \vec{v}) = \frac{\Gamma}{\rho_m}\,, \tag{2.2}$$

$$-\frac{\partial \phi}{\partial t} + \nabla \cdot \left[(1-\phi)\, \vec{V} \right] = -\frac{\Gamma}{\rho_s}\,, \tag{2.3}$$

$$\phi \left(\vec{v} - \vec{V} \right) + \frac{K}{\mu} \nabla P = 0\,, \tag{2.4}$$

$$\eta \nabla^2 \vec{V} + \left(\xi + \frac{\eta}{3} \right) \nabla \left(\nabla \cdot \vec{V} \right) - \nabla P - (\rho_s - \rho_m)\, g\, (1-\phi)\, \hat{e}_z = 0\,, \tag{2.5}$$

where ρ_m and ρ_s are the density of the melt and the solid matrix, respectively, $\vec{v}$ and $\vec{V}$ are the velocity of the melt and the solid matrix, respectively, K is the permeability of the solid matrix as described by eq. (2.1), $P = p_m + \rho_m g z$ is the modified pressure, p_m is the pressure of the melt, μ is the viscosity of the melt, ξ and η are the bulk viscosity and the shear viscosity of the solid matrix, respectively, g is the gravitational acceleration, and $\hat{e}_z$ is the unit vector in the vertical upward direction. For simplicity, we further assume that ρ_m, ρ_s, μ, ξ, and η are all constants. Γ is the melting rate, i.e., the mass exchange from the solid matrix to the melt per unit volume per unit time.

Eq. (2.2) and (2.3) are conservation of mass for melt and solid matrix, respectively. Eq. (2.4) is Darcy's law relating the modified pressure and the relative motion between the melt and the solid matrix. Eq. (2.5) is the balance of forces for the matrix involving the pressure gradient, a buoyancy term, and the deformation of the matrix itself. Notice that the inertial terms associated with the motion of the solid matrix are all neglected in this equation because we assume the viscosities ξ and η of the solid matrix are both very large. From eqs. (2.2) and (2.3) one can see that the existence of a non–zero Γ tends to induce the so–called "circulation", i.e., the average velocity of the two phases, in the system. For most of the materials in this paper, we take $\Gamma = 0$. For the cases where $\Gamma \neq 0$, we assume that Γ can be prescribed (and thus we call it "passive" melting rate hereafter) and only play a minor role in inducing flow.

It can be clearly seen from eq. (2.5) that for an initially stationary system, buoyancy effect due to density difference is the driving factor for the establishment of the pressure

field, which eventually induces the relative motion between the melt and the solid matrix. For problems like those of magma segregation we have $\rho_s > \rho_m$. However, in general this is not necessarily always the case. For example, when we apply the above governing equations to the drainage problem, where the melt phase is a normal liquid while the matrix phase is made of bubbles, we will see that $\rho_s < \rho_m$. Fortunately, one can prove that, in the case of $\rho_s < \rho_m$, the corresponding solutions ϕ, $\vec{v}$, $\vec{V}$, and P can all be related to the solution ϕ^*, $\vec{v}^*$, $\vec{V}^*$, and P^* of the following associated problem

$$\frac{\partial \phi}{\partial t} + \nabla\cdot(\phi\vec{v}) = \frac{\tilde{\Gamma}}{\rho_m}\,,$$

$$-\frac{\partial \phi}{\partial t} + \nabla\cdot\left[(1-\phi)\,\vec{V}\right] = -\frac{\tilde{\Gamma}}{\rho_s}\,,$$

$$\phi\left(\vec{v} - \vec{V}\right) + \frac{K}{\mu}\nabla P = 0\,,$$

$$\eta\nabla^2\vec{V} + \left(\xi + \frac{\eta}{3}\right)\nabla\left(\nabla\cdot\vec{V}\right) - \nabla P - (\rho_m - \rho_s)\,g\,(1-\phi)\,\hat{e}_z = 0\,,$$

in the fashion where

$$\begin{cases} \phi(x,y,z,t) = \phi^*(x,-y,-z,t)\,, \\ \vec{v}(x,y,z,t) = (u^*(x,-y,-z,t), -v^*(x,-y,-z,t), -w^*(x,-y,-z,t))\,, \\ \vec{V}(x,y,z,t) = (U^*(x,-y,-z,t), -V^*(x,-y,-z,t), -W^*(x,-y,-z,t))\,, \\ P(x,y,z,t) = P^*(x,-y,-z,t)\,, \end{cases}$$

and $\tilde{\Gamma}(x,y,z,t) = \Gamma(x,-y,-z,t)$. In other words, the case where $\rho_s < \rho_m$ is mathematically equivalent to the case where $\rho_s > \rho_m$. Therefore, without any loss of generality, we will study the case of $\rho_s > \rho_m$ only hereafter.

In the case of $\rho_s > \rho_m$, one can define the dimensionless variables ϕ', K', $\vec{v}'$, $\vec{V}'$, P',

Γ', $\vec{x}'$ (position vector), and t' as given below:

$$\left.\begin{aligned}
&\phi = \phi_0 \phi' \,, \\
&K = K_0 K' \,, \\
&\left(\vec{v}, \vec{V}\right) = \frac{K_0}{\phi_0 \mu} \left(\rho_s - \rho_m\right) g \left(\vec{v}', \vec{V}'\right) \,, \\
&P = \left(\rho_s - \rho_m\right) g \sqrt{\frac{K_0}{\mu}\left(\xi + \frac{4}{3}\eta\right)}\, P' \,, \\
&\Gamma = \left(\rho_s - \rho_m\right)^2 g \left(\sqrt{\frac{\mu}{K_0}\left(\xi + \frac{4}{3}\eta\right)}\right)^{-1} \Gamma' \,, \\
&\vec{x} = \sqrt{\frac{K_0}{\mu}\left(\xi + \frac{4}{3}\eta\right)}\, \vec{x}' \,, \\
&t = \frac{\phi_0}{\left(\rho_s - \rho_m\right) g} \sqrt{\frac{\mu}{K_0}\left(\xi + \frac{4}{3}\eta\right)}\, t' \,.
\end{aligned}\right\} \tag{2.6}$$

Notice that $\rho_s > \rho_m$ is needed here to ensure the positive value of the time scale. Here the length scale and the velocity scale are also called "compaction length" and "percolation velocity", respectively in the literature. According to Spiegelman [5], the compaction length is the scale over which the viscous resistance to volume change becomes significant, and the percolation velocity is the melt velocity in a system with uniform porosity ϕ_0 and a stationary matrix. From the typical values of all the parameters (see Table 1) one can see that the compaction is a very slow motion on a fairly large length scale.

Variable	Meaning	Typical value	Dimension
g	gravitational acceleration	9.81	$\mathrm{m/s^2}$
ϕ_0	reference porosity	0.005 – 0.1	none
ρ_s	density of solid matrix	3.3×10^3	$\mathrm{Kg/m^3}$
ρ_m	density of melt	2.8×10^3	$\mathrm{Kg/m^3}$
μ	shear viscosity of melt	1 – 10 [5]	Pa s
ξ	bulk viscosity of solid matrix	10^{18} – 10^{21} [5]	Pa s
η	shear viscosity of solid matrix	10^{18} – 10^{21} [5]	Pa s
K_0	permeability of solid matrix	10^{-16} – 10^{-12}	$\mathrm{m^2}$
$\frac{K_0}{\phi_0 \mu}\left(\rho_s - \rho_m\right) g$	percolation velocity	10^{-12} – 10^{-6}	m/s
$\sqrt{\frac{K_0}{\mu}\left(\xi + \frac{4}{3}\eta\right)}$	compaction length	10^1 – 10^4	m
$\frac{\phi_0}{\left(\rho_s - \rho_m\right) g}\sqrt{\frac{\mu}{K_0}\left(\xi + \frac{4}{3}\eta\right)}$	time scale	10^7 – 10^{16}	s

Table 1: Typical values of the parameters

Equations (2.2)−(2.5) can then be non-dimensionalized according to eq. (2.6). By dropping the primes of the dimensionless variables, the following non–dimensional equa-

tions are obtained:

$$\frac{\partial \phi}{\partial t} + \nabla \cdot (\phi \vec{v}) = (\rho_r - 1)\,\Gamma\,, \tag{2.7}$$

$$-\frac{\partial \phi}{\partial t} + \nabla \cdot \left[\left(\frac{1}{\phi_0} - \phi \right) \vec{V} \right] = -\left(1 - \frac{1}{\rho_r} \right) \Gamma\,, \tag{2.8}$$

$$\left(\vec{v} - \vec{V} \right) + \phi^{n-1} \nabla P = 0\,, \tag{2.9}$$

$$\nabla \left(\nabla \cdot \vec{V} \right) - \beta \nabla \times \left(\nabla \times \vec{V} \right) - \phi_0 \nabla P - \phi_0 \left(1 - \phi_0 \phi \right) \hat{e}_z = 0\,, \tag{2.10}$$

where $\rho_r = \dfrac{\rho_s}{\rho_m} > 1$ is the density ratio, and $\beta = \dfrac{\eta}{\xi + \dfrac{4}{3}\eta} < \dfrac{3}{4}$ is the viscosity ratio.

For mathematical convenience, we restrict our attention to the case where the reference (background) porosity ϕ_0 is very small so that we can express the solutions in terms of a power series in ϕ_0 as follows:

$$\left.\begin{aligned} \phi &= \phi^{(0)} + \phi_0 \phi^{(1)} + \cdots \\ \vec{v} &= \vec{v}^{(0)} + \phi_0 \vec{v}^{(1)} + \cdots \\ \vec{V} &= \phi_0 \vec{V}^{(0)} + \phi_0^2 \vec{V}^{(1)} + \cdots \\ P &= P^{(0)} + \phi_0 P^{(1)} + \cdots \end{aligned}\right\} \tag{2.11}$$

Substituting eq. (2.11) into (2.7)−(2.10) and dropping the superscript "(0)" for simplicity, one can arrive at the following equations for the leading–order fields:

$$\frac{\partial \phi}{\partial t} + \nabla \cdot (\phi \vec{v}) = (\rho_r - 1)\Gamma\,, \tag{2.12}$$

$$-\frac{\partial \phi}{\partial t} + \nabla \cdot \vec{V} = -\left(1 - \frac{1}{\rho_r} \right) \Gamma\,, \tag{2.13}$$

$$\vec{v} + \phi^{n-1} \nabla P = 0\,, \tag{2.14}$$

$$\nabla \left(\nabla \cdot \vec{V} \right) - \beta \nabla \times \left(\nabla \times \vec{V} \right) - \nabla P - \hat{e}_z = 0\,. \tag{2.15}$$

By taking the curl of eq. (2.15) we have

$$\nabla \times \left[\nabla \times \left(\nabla \times \vec{V} \right) \right] = 0 \quad \Longrightarrow \quad \nabla^2 \left(\nabla \times \vec{V} \right) = 0\,. \tag{2.16}$$

For further simplification, we follow Barcilon & Lovera[6] and assume that the domain is infinite and the motion is confined, thus $\nabla \times \vec{V} = 0$ at infinity. This, combined with

eq. (2.16), leads to $\nabla \times \vec{V} = 0$ everywhere in the domain. Therefore eq. (2.15) can be reduced to

$$\nabla\Big(\nabla \cdot \vec{V}\Big) - \nabla P - \hat{e}_z = 0 \tag{2.17}$$

and

$$\nabla \times \vec{V} = 0\,.$$

Now, by eliminating P, $\vec{v}$, and $\vec{V}$ from eqs. (2.12)−(2.14) and (2.17) one can obtain a single nonlinear equation for ϕ as given below:

$$\begin{aligned} -\frac{\partial \phi}{\partial t} + (\rho_r - 1)\Gamma + \phi^n \nabla^2\left(\frac{\partial \phi}{\partial t}\right) + n\phi^{n-1}\nabla\phi \cdot \nabla\left(\frac{\partial \phi}{\partial t}\right) - \left(1 - \frac{1}{\rho_r}\right)\phi^n \nabla^2\Gamma \\ -n\left(1 - \frac{1}{\rho_r}\right)\phi^{n-1}\nabla\phi \cdot \nabla\Gamma - n\phi^{n-1}\frac{\partial \phi}{\partial z} = 0 \end{aligned} \tag{2.18}$$

We note that when $\Gamma = 0$ and $n = 3$, this equation becomes essentially the same nonlinear evolution equation for ϕ derived by Barcilon & Lovera[6].

3 Wave Solution

In their pioneering paper, Barcilon & Richter[1] carried out numerical investigations and showed from their numerical results that in one–dimensional systems, an arbitrary initial profile $\phi(z, 0)$ eventually breaks up into a series of waves as time goes by. Since then, considerable work has been done on the nonlinear waves in the two–phase system (see Spiegelman[7] for a review). Later Wiggins & Spiegelman[8] suggested that the existence of waves in such systems depends only on the conditions that the matrix is permeable and viscously deformable. If their claim is true, then waves always exist in the system formulated earlier in section 2. Furthermore, since the buoyancy effect is the driving force of the flow, it would be natural to assume that waves mainly, if not only, propagate in the z–direction.

To capture the waves propagating in the z–direction, one can introduce a frame $\zeta = z - ct$ which moves with the waves, where c is the prescribed wave speed. Since waves generally take on the form $\phi = \phi(x, y, \zeta)$, eq. (2.18) then becomes

$$\begin{aligned} c\phi_\zeta + (\rho_r - 1)\,\Gamma - c\phi^n \nabla^2\phi_\zeta - nc\phi^{n-1}\nabla\phi \cdot \nabla\phi_\zeta - \left(1 - \frac{1}{\rho_r}\right)\phi^n \nabla^2\Gamma \\ -n\left(1 - \frac{1}{\rho_r}\right)\phi^{n-1}\nabla\phi \cdot \nabla\Gamma - n\phi^{n-1}\phi_\zeta = 0\,, \end{aligned} \tag{3.1}$$

where $\phi_\zeta = \dfrac{\partial \phi}{\partial \zeta}$, and $\nabla = \hat{e}_x \dfrac{\partial}{\partial x} + \hat{e}_y \dfrac{\partial}{\partial y} + \hat{e}_z \dfrac{\partial}{\partial \zeta}$. In addition, following Barcilon & Lovera[6], we only look for solutions of eq. (3.1) such that

$$\phi - 1,\ |\nabla \phi|\,,\ |\nabla \phi_\zeta| \in L_2(\mathcal{R}) \tag{3.2}$$

and $\phi > 0$. Inclusion of these conditions brings additional limitations for the wave speed c. For example, Barcilon & Lovera[6] proved that, under the conditions that $n = 3$ and no melting effect, $c > 0$ if a solution of eq. (3.1) exists. Furthermore, $c > 3$ is needed to ensure the integrability of the conserved quantities. In fact, using the same approach as theirs, one can prove that, in case n takes on any positive value other than 3, $c > 0$ is still needed in order for the solution to exist, while $c > n$ is needed to ensure the integrability.

With regard to the boundary conditions for the wave solution, since we consider the flow in an infinite domain, it is reasonable to assume that the outer boundary, i.e., the one at infinity, is not affected by the wave propagation. In other words, at the outer boundary the porosity is always equal to 1. On the other hand, if all the boundary conditions are proposed at the outer boundary, then because of the uniformity of the porosity at the outer boundary one cannot get any solution of eq. (3.1) other than $\phi = 1$, which is the trivial solution of eq. (3.1). Therefore, in order to obtain a non-trivial solution, one must propose some boundary conditions somewhere inside the domain, which is called "inner boundary" hereafter, to indicate how the porosity disturbance is introduced.

Intuitively one may think that specifying the porosity value at the location where the porosity disturbance is introduced is appropriate because such a condition represents the strength of the disturbance and can be directly determined by how the disturbance is introduced. However, this is not true, and the reason is that the wave solution is not valid for all the time after the introduction of the disturbance. To illustrate this point, let us consider an arbitrary porosity disturbance $\delta\phi(x, y, z)$ superposed onto $\phi = 1$ at $t = t^*$. If the wave solution is valid for all time $t > t^*$, then the porosity profile at any time $t > t^*$ is simply $1 + \delta\phi(x, y, z - ct)$. However, this is not necessarily a solution of eq. (3.1). In fact, right after an arbitrary disturbance is applied the system starts to undergo a transition process, in which the disturbance diffuses and affects more and more space. For example, in case that there's no phase change ($\Gamma = 0$) between the two phases, the volume occupied by the melt in a selected domain $\mathcal{R}$ should not change with time, i.e.

$$\frac{\mathrm{d}}{\mathrm{d}t} \int_{\mathcal{R}} \phi(x, y, z, t)\, \mathrm{d}V = 0\,. \tag{3.3}$$

Only after the transition process is done the wave solution is possibly valid. Therefore, even though we may know how the porosity disturbance is introduced we may not know

the porosity value at the inner boundary without solving for the transition process. In this sense, specifying the porosity value at the inner boundary is not an appropriate boundary condition for the wave equation. Under this circumstance, the possible candidates of the inner boundary conditions are the conditions about the spatial derivatives of the porosity. We will discuss more about the inner boundary conditions in the next section.

4 Similarity Wave Solution

4.1 Existence Conditions for Similarity Waves

We now restrict our focus to the similarity wave solutions of eq. (3.1) in the form of $\phi = \phi(s)$, where s is the similarity variable defined as $s = s(x, y, \zeta)$. We further require $s_\zeta = \dfrac{\partial s}{\partial \zeta} \neq 0$ so that the wave behavior is preserved in the solution. Eq. (3.1) is then converted into

$$\begin{aligned} & cs_\zeta \phi_s + (\rho_r - 1)\Gamma - c\phi^n \left[s_\zeta \left(s_x^2 + s_y^2 + s_\zeta^2 \right) \phi_{sss} + 2 \left(s_x s_{x\zeta} + s_y s_{y\zeta} + s_\zeta s_{\zeta\zeta} \right) \phi_{ss} \right. \\ & \quad \left. + s_\zeta \left(s_{xx} + s_{yy} + s_{\zeta\zeta} \right) \phi_{ss} + \left(s_{xx\zeta} + s_{yy\zeta} + s_{\zeta\zeta\zeta} \right) \phi_s \right] - nc\phi^{n-1} \left[s_\zeta \left(s_x^2 + s_y^2 + s_\zeta^2 \right) \phi_s \phi_{ss} \right. \\ & \quad \left. + \left(s_x s_{x\zeta} + s_y s_{y\zeta} + s_\zeta s_{\zeta\zeta} \right) \phi_s^2 \right] - ns_\zeta \phi^{n-1} \phi_s - n \left(1 - \frac{1}{\rho_r} \right) \left(s_x \Gamma_x + s_y \Gamma_y + s_\zeta \Gamma_z \right) \phi^{n-1} \phi_s \\ & \quad - \left(1 - \frac{1}{\rho_r} \right) \left(\Gamma_{xx} + \Gamma_{yy} + \Gamma_{zz} \right) \phi^n = 0 \,. \end{aligned} \tag{4.1}$$

It is clear that in order to have similarity solutions, the following conditions need to be satisfied:

$$\begin{cases} a) \quad \Gamma = f_1(s) s_\zeta \\ b) \quad s_x^2 + s_y^2 + s_\zeta^2 = f_2(s) \\ c) \quad s_x s_{x\zeta} + s_y s_{y\zeta} + s_\zeta s_{\zeta\zeta} = f_3(s) s_\zeta \\ d) \quad s_{xx} + s_{yy} + s_{\zeta\zeta} = f_4(s) \\ e) \quad s_{xx\zeta} + s_{yy\zeta} + s_{\zeta\zeta\zeta} = f_5(s) s_\zeta \\ f) \quad s_x \Gamma_x + s_y \Gamma_y + s_\zeta \Gamma_z = f_6(s) s_\zeta \\ g) \quad \Gamma_{xx} + \Gamma_{yy} + \Gamma_{zz} = f_7(s) s_\zeta \end{cases} \tag{4.2}$$

where $f_1(s) - f_7(s)$ are arbitrary functions of s. By observation one can see that as long as a), b), and d) are satisfied, the remaining four conditions will also be satisfied. In fact,

the following relations hold for the functions $f_1(s) - f_7(s)$:

$$\begin{cases} f_3 = \dfrac{1}{2} f_2' \\ f_5 = f_4' \\ f_6 = f_1 f_3 + f_1' f_2 = \dfrac{1}{2} f_1 f_2' + f_1' f_2 = \dfrac{\left(f_1^2 f_2\right)'}{2 f_1} \\ f_7 = (f_1 f_4)' + \dfrac{\left(f_1' f_2^2\right)'}{f_2} \end{cases} \tag{4.3}$$

Once the conditions in eq. (4.2) are all satisfied, the equation for ϕ becomes

$$\begin{aligned} & c\phi_s + (\rho_r - 1) f_1 - c\phi^n \left[f_2 \phi_{sss} + (2 f_3 + f_4) \phi_{ss} + f_5 \phi_s \right] - nc\phi^{n-1} \left(f_2 \phi_s \phi_{ss} + f_3 \phi_s^2 \right) \\ & - n\phi^{n-1}\phi_s - n \left(1 - \frac{1}{\rho_r} \right) f_6 \phi^{n-1} \phi_s - \left(1 - \frac{1}{\rho_r} \right) f_7 \phi^n = 0 \,. \end{aligned} \tag{4.4}$$

In the remainder of this paper, we study only the following form of $s = s(x, y, \zeta)$:

$$s^m = a x^m + b y^m + \zeta^m \tag{4.5}$$

where $m > 0$, a and b are constants. In this case, there are only two possibilities for conditions b) and d) in eq. (4.2) to be satisfied:

a) $m = 1$:
In this case $s = ax + by + \zeta$, $f_2 = a^2 + b^2 + 1$, and $f_3 = f_4 = f_5 = 0$. Hereafter we call this case as the "linear case".

b) $m = 2$ while a and b are either 0 or 1:
In this case $s^2 = ax^2 + by^2 + \zeta^2$, $f_2 = 1$, $f_3 = 0$, $f_4 = \dfrac{a+b}{s}$, and $f_5 = -\dfrac{a+b}{s^2}$. Hereafter we call this case as the "quadratic case". It actually contains two subcases:

   (i) Only one out of a and b is 1, i.e., $s^2 = x^2 + \zeta^2$ or $s^2 = y^2 + \zeta^2$. This is referred to as "cylindrical case" by Barcilon & Lovera[6].

   (ii) Both a and b are 1, i.e., $s^2 = x^2 + y^2 + \zeta^2$. This is referred to as "spherical case" by Barcilon & Lovera[6].

   The "$a = b = 0$" subcase is not considered in this case since it is the same as "$a = b = 0$" subcase for the linear case.

4.2 Boundary Conditions

Here we would like to examine the behavior of the similarity waves between the inner boundary (usually taken as $s = 0$) and the outer boundary ($s \to \infty$). Since eq. (4.4) is a 3^{rd}–order ODE of s, we need three boundary conditions to determine the solution. Among them the following two conditions are considered at the outer boundary to regulate the far field behavior of solution:

$$\phi \to 1, \quad \phi_s \to 0 \qquad \text{as} \qquad s \to \infty \,. \tag{4.6}$$

As we discussed in section 3, in order to determine the solution, one has to employ one condition related to the derivative(s) of the porosity as the boundary condition at the inner boundary.

By continuation we can extend the definition of ϕ and f_i's to $-\infty < s < 0$. It is easy to see that in both the linear case and the quadratic case, f_2 and f_5 are even functions of s while f_3 and f_4 are odd functions of s. It can then be observed from eq. (4.3) that, as long as f_1 is an odd function of s, eq. (4.4) admits a solution which is an even function of s. Therefore, when f_1 is an odd function (such as the melting–free case), it is fairly reasonable to use

$$\phi_s = 0 \qquad \text{at} \qquad s = 0 \tag{4.7}$$

as the inner boundary condition. When f_1 is not an odd function of s, we still use eq. (4.7). However, since in this case eq. (4.4) no longer admits an even solution in $-\infty < s < \infty$, the interpretation of eq. (4.7) is simply that we require the solution to reach a local minimum/maximum at the inner boundary. Since in our model the waves are basically induced by porosity disturbance(s) to the uniform porosity $\phi = 1$ at the inner boundary, this requirement is believed to be reasonable.

4.3 General Behavior of Similarity Waves in the Absence of Melting

Before we actually solve eq. (4.4), let us further analyze this equation to see if there are any general behavior of the solution for the melting–free ($f_1 = 0$) case. A first integral and second integral of this equation are thus needed, and they are determined using the same approach described in Barcilon & Lovera[6].

To determine the unknown constant in the first integral, we further assume

$$\phi_{ss} \to 0 \qquad \text{as} \qquad s \to \infty \,. \tag{4.8}$$

This condition actually regulates a little further the smoothness of the solution at far field, and in this sense it should be totally compatible with eq. (4.6). Furthermore, for the time being we only consider the $n = 3$ case. The effect of n on the behavior of the solution will be addressed in subsection 6.1.

4.3.1 The Linear Case

In the linear case and when $n = 3$, eq. (4.4) becomes

$$c\phi_s - c\phi^3\left(a^2+b^2+1\right)\phi_{sss} - 3c\phi^2\left(a^2+b^2+1\right)\phi_s\phi_{ss} - 3\phi^2\phi_s = 0\,, \tag{4.9}$$

which is subjected to the boundary conditions (4.6), (4.7) and (4.8). By observation, one can find the following first integral of this equation:

$$c(a^2+b^2+1)\phi^3\phi_{ss} + c(1-\phi) + (\phi^3-1) = 0\,. \tag{4.10}$$

If we multiply eq. (4.10) by ϕ_s, then divide by ϕ^3 and integrate we have the following second integral of eq. (4.9):

$$c\left(a^2+b^2+1\right)\phi_s^2 + c\left(\frac{2}{\phi} - \frac{1}{\phi^2} - 1\right) + \left(2\phi + \frac{1}{\phi^2} - 3\right) = 0\,. \tag{4.11}$$

Another useful integral can be obtained by dividing eq. (4.9) by ϕ^2 and integrating, which leads to

$$c\left(a^2+b^2+1\right)\left(\phi\phi_{ss} + \phi_s^2\right) + (\phi-1)\left(3 - \frac{c}{\phi}\right) = 0\,. \tag{4.12}$$

Based on these integrals we have the following theorems:

Theorem 1. *For $c > 3$, if the similarity wave solution exists in the linear case, then $\phi \geq 1$.*

Proof. Let us assume that ϕ can be smaller than 1 somewhere in the domain. Then, since $\phi \to 1$ at the outer boundary, it must have at least one minimum somewhere in the domain, say at $s = s_1$. At that point

$$0 < \phi(s_1) < 1, \quad \phi_s(s_1) = 0, \quad \phi_{ss}(s_1) > 0$$

and thus both terms on the left-hand side of eq. (4.12) are positive at $s = s_1$, which causes conflict. Therefore, $\phi \geq 1$ everywhere. □

Theorem 2. *For the non-trivial similarity wave solution in the linear case with $c > 3$, $\phi = 1$ can be asymptotically approached but can never be reached.*

Proof. Let us assume that $\phi = 1$ can be reached, at say $s = s_1$, in the domain. Then from eqs. (4.9), (4.10), and (4.11) we have

$$\phi_s(s_1) = \phi_{ss}(s_1) = \phi_{sss}(s_1) = 0\,.$$

Now, let us denote by N the order of the leading non–zero derivative of ϕ with respect to s at $s = s_1$. Then, $N \geq 4$ and $\phi(s)$ has the following approximation around $s = s_1$

$$\phi \sim 1 + \frac{f_N}{N!}\,(s - s_1)^N\ ,$$

where $f_N = \phi^{(N)}(s_1)$. By substituting this expression into eq. (4.9) and balancing the leading order terms, we can prove that $f_N = 0$. This way we can see that all the derivatives of ϕ with respect to s are zero at $s = s_1$ and thus $\phi = 1$ in the neighborhood of $s = s_1$. Therefore, if the solution reaches $\phi = 1$ somewhere in the domain, then $\phi = 1$ everywhere. In other words, the solution is a trivial solution. □

Theorem 3. *For the non–trivial similarity wave solution in the linear case with $c > 3$, if it ever has a local extremum on $s \in (0, \infty)$, then that extremum must be a maximum and $\phi = \dfrac{1}{2}(c-1)$ there.*

Proof. At every possible local extrema on $(0, \infty)$, say at $s = s_1$, we have

$$\phi_s(s_1) = 0\,.$$

Hence eq. (4.11) becomes

$$c\left(\frac{2}{\phi_1} - \frac{1}{\phi_1^2} - 1\right) + \left(2\phi_1 + \frac{1}{\phi_1^2} - 3\right) = 0 \quad \Longrightarrow \quad (2\phi_1 + 1 - c)\,(\phi_1 - 1)^2 = 0\,,$$

where $\phi_1 = \phi(s_1)$. Since $\phi_1 \neq 1$ (Theorem 2), we must have

$$\phi_1 = \frac{1}{2}(c-1)\,.$$

On the other hand, from eq. (4.10) we see that when $\phi_1 = \dfrac{1}{2}(c-1)$,

$$\phi_{ss}(s_1) = \frac{c(\phi_1 - 1) - (\phi_1^3 - 1)}{c\left(a^2 + b^2 + 1\right)\phi_1^3} = -\frac{(\phi_1 - 1)(c-3)(c-1)}{4c\left(a^2 + b^2 + 1\right)\phi_1^3} < 0\,.$$

Therefore, $\phi_1 = \dfrac{1}{2}(c-1)$ is the local maximum. □

In fact, Theorem 3 implies two main results. First, there's no local minimum in $(0, \infty)$, and hence the solution can only be either monotonically decreasing function of s or there is only one local maximum within $(0, \infty)$. Second, for our boundary condition selection, $\phi(s = 0)$ reaches $\frac{1}{2}(c - 1)$, which is the possible maximum. Combining these two results, one can further have the following theorem.

Theorem 4. *For $c > 3$, if the similarity wave solution exists in the linear case, it is a monotonically decreasing function of s.*

Proof. Let us assume that the solution is not monotonically decreasing. Then ϕ must have exactly one local maximum, at say $s = s_1 > 0$, such that ϕ increases with s when $0 \leq s \leq s_1$ and decreases with s when $s > s_1$. However, this is not possible since ϕ already reaches the possible maximum at $s = 0$. Therefore, the solution must be monotonically decreasing with s. □

4.3.2 The Cylindrical Case

In the cylindrical case and when $n = 3$, eq. (4.4) becomes

$$c\phi_s - c\phi^3\left(\phi_{sss} + \frac{1}{s}\phi_{ss} - \frac{1}{s^2}\phi_s\right) - 3c\phi^2\phi_s\phi_{ss} - 3\phi^2\phi_s = 0 \tag{4.13}$$

subjected to the boundary conditions (4.6), (4.7) and (4.8). From Bariclon & Lovera[6] we have the following integrals of this equation:

$$c\phi^3\left(\phi_{ss} + \frac{1}{s}\phi_s\right) + 3\int_s^\infty \frac{1}{r}\phi^2\phi_r^2\,\mathrm{d}r = c(\phi - 1) - (1 - \phi^3)\,, \tag{4.14}$$

$$c\phi_s^2 + c\int_s^\infty \phi_r^2\left[1 - 3\frac{\phi^2}{\phi^2(s)}\right]\frac{\mathrm{d}r}{r} = \frac{(\phi - 1)^2}{\phi^2}(c - 1 - 2\phi)\,, \tag{4.15}$$

$$c\left(\phi\phi_{ss} + \phi_s^2 + \frac{1}{s}\phi\phi_s\right) + c\int_s^\infty \frac{1}{r}\phi_r^2\,\mathrm{d}r + (\phi - 1)\left(3 - \frac{c}{\phi}\right) = 0\,, \tag{4.16}$$

where eq. (4.14) is a first integral of eq. (4.13), and eq. (4.15) is a second integral of eq. (4.13). As we can see here, unlike the linear case, in the cylindrical case (and the upcoming spherical case too) neither $|\phi_s|$ nor ϕ_{ss} solely depends on the local value of ϕ. Based on these integrals we have the following theorems:

Theorem 5. *For $c > 3$, if the similarity wave solution exists in the cylindrical case, then $\phi \geq 1$.*

This theorem has been proved by Barcilon & Lovera[6].

Theorem 6. *For the non–trivial similarity wave solution in the cylindrical case with $c > 3$, $\phi = 1$ can be asymptotically approached but can never be reached.*

Proof. Let us assume that a solution reaches $\phi = 1$, at say $s = s_1$, in the domain. Firstly, $\phi_s(s_1) = 0$, otherwise at either s_1^- or s_1^+ there is $\phi < 1$, which contradicts Theorem 6. Secondly, $\phi_{ss}(s_1) = 0$. This is because that $\phi_{ss}(s_1) < 0$ leads to $\phi < 1$ at both s_1^- and s_1^+, while $\phi_{ss}(s_1) > 0$ leads to contradiction to eq.(4.14) at $s = s_1$. Thirdly, based on eq. (4.13), $\phi_{sss}(s_1) = 0$.

Now we perform a Taylor–series expansion of ϕ at $s = s_1$, then apply it to eq. (4.13) and balance the leading order terms. This way we can prove that all the derivatives of ϕ with respect to s are zero at $s = s_1$. In other words, $\phi = 1$ in the neighborhood of $s = s_1$. Therefore, if the solution reaches $\phi = 1$ somewhere in the domain, then $\phi = 1$ everywhere, namely, the solution is a trivial solution. □

Theorem 7. *For $c > 3$, if the similarity wave solution exists in the cylindrical case, then there's no local minimum in the solution.*

Proof. Let us assume that the solution has at least one local minimum point at say $s = s_1$. The value of ϕ at this point, say ϕ_1, is greater than 1 because of Theorem 5. Since $\phi \to 1$ as $s \to \infty$, there is another point, say $s = s_2 > s_1$, where ϕ has the same value ϕ_1 and

$$\phi(s) \geq \phi_1 \quad \text{for } s \in (s_1, s_2)\,.$$

Now, if we evaluate eq. (4.15) at both s_1 and s_2 and then subtract the resultant equations, we find that

$$-\phi_s^2(s_2) + \int_{s_1}^{s_2} \left[1 - 3\frac{\phi^2(r)}{\phi_1^2}\right] \frac{\mathrm{d}r}{r} = 0\,,$$

which is impossible since the left-hand side is negative definite. □

In fact, Theorem 7 leads to an important conclusion that the solution is a monotonically decreasing function of s. If this is not true, then because of this theorem, the solution has one and only one local maximum at say $s = s_1$ such that ϕ increases with s when $0 \leq s \leq s_1$ and it decreases with s when $s > s_1$. However, this makes $s = 0$ a local minimum, which contradict this theorem.

Now that the maximum value of ϕ, denoted by ϕ_0, is at $s = 0$, we would like to figure out how ϕ_0 is related to the wave speed c, just like what we investigated in the linear case.

To do that, we evaluate eq. (4.15) at $s = 0$ to obtain

$$c\int_0^\infty \phi_r^2\left[1-3\frac{\phi^2}{\phi_0^2}\right]\frac{\mathrm{d}r}{r} = \frac{(\phi_0-1)^2}{\phi_0^2}(c-1-2\phi_0)\,.$$

At this time, we can not tell for sure the sign of the above integral. However, since $\frac{1}{r}$ is a decaying factor, it's quite possible that the bulk part of this integral is captured in the term

$$c\int_0^\Delta \phi_r^2\left[1-3\frac{\phi^2}{\phi_0^2}\right]\frac{\mathrm{d}r}{r}\,,$$

where Δ is a limited positive value such that $\phi(s) \geq \frac{1}{\sqrt{3}}\phi_0$ for all $0 \leq s \leq \Delta$. If this speculation is true, then we have

$$\frac{(\phi_0-1)^2}{\phi_0^2}(c-1-2\phi_0) < 0$$

which yields $\phi_0 > \frac{1}{2}(c-1)$.

4.3.3 The Spherical Case

In the spherical case and when $n = 3$, eq. (4.4) becomes

$$c\phi_s - c\phi^3\left(\phi_{sss}+\frac{2}{s}\phi_{ss}-\frac{2}{s^2}\phi_s\right) - 3c\phi^2\phi_s\phi_{ss} - 3\phi^2\phi_s = 0 \tag{4.17}$$

subjected to the boundary conditions (4.6), (4.7) and (4.8). Using the same approach described in Bariclon & Lovera[6], one can obtain the following integrals of this equation:

$$c\phi^3\left(\phi_{ss}+\frac{2}{s}\phi_s\right) + 6\int_s^\infty \frac{1}{r}\phi^2\phi_r^2\,\mathrm{d}r = c(\phi-1)-(1-\phi^3)\,, \tag{4.18}$$

$$c\phi_s^2 + 2c\int_s^\infty \phi_r^2\left[1-3\frac{\phi^2}{\phi^2(s)}\right]\frac{\mathrm{d}r}{r} = \frac{(\phi-1)^2}{\phi^2}(c-1-2\phi)\,, \tag{4.19}$$

$$c\left(\phi\phi_{ss}+\phi_s^2+\frac{2}{s}\phi\phi_s\right) + c\int_s^\infty \frac{2}{r}\phi_r^2\,\mathrm{d}r + (\phi-1)\left(3-\frac{c}{\phi}\right) = 0\,, \tag{4.20}$$

where eqs. (4.18) and (4.19) are a first integral and a second integral of eq. (4.17), respectively. Similar to the cylindrical case, we have the following theorems based on these integrals:

Theorem 8. *For $c > 3$, if the similarity wave solution exists in the spherical case, then $\phi \geq 1$.*

Theorem 9. *For the non–trivial similarity wave solution in the spherical case with $c > 3$, $\phi = 1$ can be asymptotically approached but can never be reached.*

Theorem 10. *For $c > 3$, if the similarity wave solution exists in the spherical case, it has no local minimum point.*

All these theorems can be proved in exactly the same manner as what is applied in proving their equivalents in the cylindrical case. Once again, Theorem 10 leads to the conclusion that the solution is a monotonically decreasing function of s, and we suspect that the maximum porosity is greater than $\frac{1}{2}(c-1)$.

5 Numerical Result

Numerical schemes are used to determine the solutions for various cases studied in this paper. In this section, we shall only present the baseline results, i.e., results for the $n = 3$ and $\Gamma = 0$ case. The results for $n \neq 3$ and $\Gamma \neq 0$ will be presented and compared with the baseline results in the next section.

5.1 The Linear Case

In the linear case, the first integral (4.10) turns the original 3^{rd}–order system (4.9) into the following 2^{nd}–order system:

$$c(a^2 + b^2 + 1)\phi^3\phi_{ss} + c(1-\phi) + (\phi^3 - 1) = 0\,.$$

As we can see here, parameters $\lambda \equiv a^2 + b^2 + 1$ and c govern the solution. In other words, solution depends on λ and not on a or b individually. As to the two boundary conditions needed for solving this ODE, normally we use "$\phi_s(s = 0) = 0$" and a condition at the outer boundary. However, because of Theorem 3, the condition $\phi = \frac{1}{2}(c-1)$ at the inner boundary can be used to replace the outer condition. This way all the boundary conditions are posed at the same boundary, so that a forward integration using the 4^{th}–order Runge–Kutta method can be used to solve the governing system.

Numerical solutions for different values of c and λ are determined to see how these two parameters affect the solution. For each solution, we trace the variation of ϕ with s to determine the location of the outer edge, defined as the location where $\phi = 1 + 10^{-5}$. The span of the solution, defined as the distance from the inner boundary ($s = 0$) to the outer edge and denoted by L, can then be determined. This span can be interpreted as

the size of the zone influenced by the wave propagation. In our study, we examine the variation of L with λ and c.

Typical porosity profiles of the similarity waves are shown in Figure 2, which also indicates how the profiles vary with the wave speed c. It can be seen that, while all the solutions have qualitatively the same shape, the solution with a faster wave speed is everywhere greater than the solution for ϕ with a slower wave speed. Profiles corresponding to different values of λ are plotted in Figure 3, which shows that the solution corresponding to a greater value of λ is everywhere greater than the solution with a smaller value of λ. Typical phase diagram of the solution is shown in Figure 4 as the solid line. It is observed that ϕ_s is always negative, and it has one and only one minimum somewhere within the domain. The evolution of ϕ with s is along the phase diagram, from the top end to the bottom end. Also shown in this figure as the dashed line is the variation of ϕ_{ss} versus ϕ_s. It shows that ϕ_{ss} starts with a negative value at $s = 0$, and it keeps increasing with s until reaching a positive maximum somewhere after the minimum point of ϕ_s, where ϕ_{ss} reaches zero. After that, ϕ_{ss} decreases with s and goes to zero as it approaches to the outer edge. On this curve, the evolution of the system is from the bottom end to the top end.

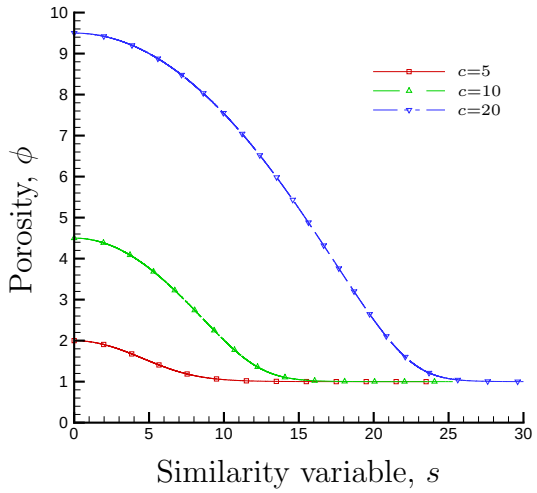

Figure 2: Profiles of the similarity waves in the linear case versus wave speed ($\lambda = 1$)

We also carried out studies about how the span of linear similarity waves varies with respect to c and λ. The results regarding the dependence of the span on the wave speed c

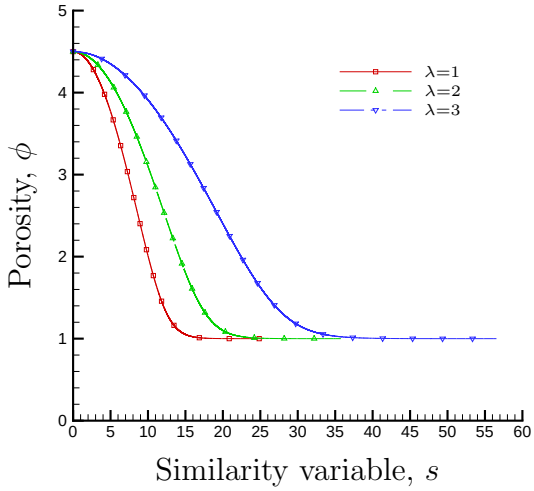

Figure 3: Profiles of the similarity waves in the linear case versus λ ($c = 10$)

will be shown together with the corresponding results from the quadratic case for the purpose of comparison between the results for the linear case and the quadratic cases. The dependence of the span on λ for $c = 10$, on the other hand, is shown in Figure 5. It can be seen that at least for this particular wave speed, the span monotonically increases with λ, while the rate of increase $\dfrac{\mathrm{d}L}{\mathrm{d}\lambda}$ seems gradually decrease as λ increases.

5.2 The Quadratic Case

Compared with the linear case, determination of the solution for the quadratic cases is much more complicated. First, the first integral (eq. (4.14) and eq. (4.18), respectively) no longer expresses ϕ_{ss} as an algebraic combination of ϕ and ϕ_s, and thus instead of solving a 2^{nd}–order system, we have to solve the original 3rd–order system. Second, $s = 0$ is a singularity point, and we have to consider the neighborhood of $s = 0$ separately. The way we deal with it is to apply the inner boundary condition at $s = \delta \ll 1$ and assume the solution is uniform for $0 \leq s \leq \delta$. Finally, since we do not know for sure the value of ϕ at $s = 0$, it is impossible to place all the 3 boundary conditions at the inner boundary. This means a simple forward integration can not solve the problem. Instead, a shooting method is needed to determine the solution.

The first step of determining the solution is to determine the far field asymptotic

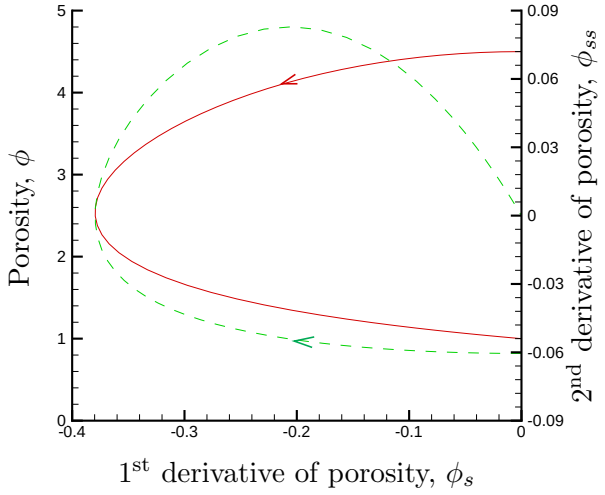

Figure 4: Phase diagram for similarity wave in the linear case ($c = 10$ and $\lambda = 1$). Here the solid line presents ϕ versus ϕ_s, while the dashed line presents ϕ_{ss} versus ϕ_s.

solution. To do this, we expand the solution in the far field as

$$\phi(s) = 1 + \psi(s) + \cdots , \tag{5.1}$$

where $\psi(s) \ll 1$ as $s \to \infty$. Then both eq. (4.13) and eq. (4.17) become

$$c\psi_{sss} + (3 - c)\psi_s = 0 , \tag{5.2}$$

which leads to an exponentially decaying solution of ψ in the far field in the form

$$\psi \sim e^{-ks} , \tag{5.3}$$

where $k = \sqrt{\dfrac{c-3}{c}}$ is the decaying rate. It can be observed that for the same wave speed, the solution decays at the same rate in the far field, for both the cylindrical and the spherical case. In fact, by applying the same approach to eq. (4.9), one can obtain in the linear case

$$\psi \sim e^{-ks} \quad \text{with } k = \sqrt{\frac{c-3}{c\lambda}} . \tag{5.4}$$

Since $\lambda = a^2 + b^2 + 1 \geq 1$, for the same wave speed, a wave in the linear case generally decays more slowly than its counterparts in the quadratic cases.

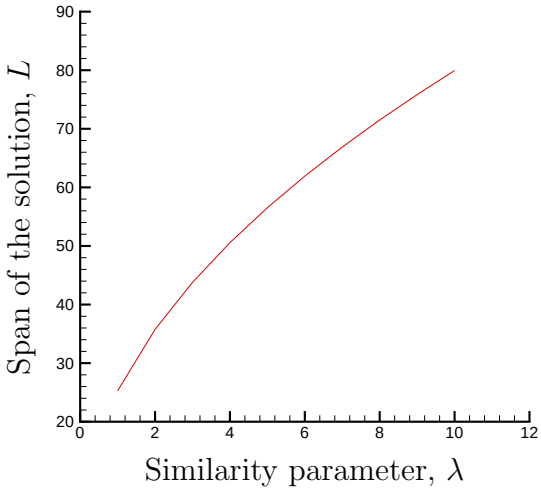

Figure 5: Span of the linear similarity waves versus λ ($c = 10$)

Once we obtain the far field solution, we can apply the following boundary conditions to start a 4^{th}–order Runge–Kutta backward integration towards $s = \delta$

$$\phi = 1 + \epsilon, \quad \phi_s = -k\epsilon, \quad \phi_{ss} = k^2\epsilon \qquad \text{at} \quad s = s_\infty \,, \tag{5.5}$$

where $\epsilon = 10^{-5}$, and s_∞ is a constant to be determined. A shooting method is employed to adjust the value of s_∞ until $|\phi_s(s = \delta)| < 10^{-6}$.

Using the above approach, we obtained the solutions for both cylindrical and spherical cases using several different values of the wave speed. Typical porosity profiles of the solutions are shown in Figure 6. The solution for the linear case with $\lambda = 1$ is also provided for comparison. It can be clearly seen that for the same wave speed, the spherical case has the largest amplitude everywhere, while the linear case with $\lambda = 1$ shows the lowest amplitude. The shapes, on the other hand, are qualitatively similar. Particularly, the maximum porosity does exceed $\dfrac{c-1}{2}$, as we speculated earlier in the previous section.

Typical phase diagram for the cylindrical case and the spherical case are plotted in Figures 7 and 8, respectively. It can be observed that the shapes of the phase diagrams are similar to those for the linear case. However, since the inner boundary is a regular point in the linear case while it is a singularity in the quadratic cases, it is expected that the behavior of the solution around the inner boundary is quite different for the linear case and for the quadratic cases. In fact, significant difference between the linear case (Figure 4) and the quadratic cases does exist around the inner boundary.

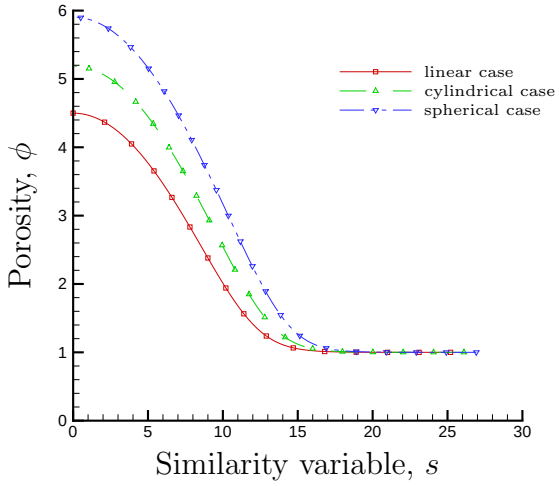

Figure 6: Profiles of the similarity wave in different cases ($c = 10$)

To gain a better understanding of how the behavior of the solutions vary with the wave speed, we investigated the variation of maximum porosity and the span of the solution. The results are shown in Figures 9 and 10, respectively. It can be seen that in all the three cases, the maximum porosity increases with the wave speed. While such increase follows a linear relationship in the linear case, it doesn't always follow a linear relationship in the quadratic cases, especially when the wave speed is small, say for $c \leq 7$. With regard to the variation of span, it can be seen that the span decreases with the wave speed when the wave speed is small, and it increases with the wave speed when the wave speed becomes large. Very interestingly, the minimum span for all the three cases occurs at about $c = 5.5$.

6 Parametric Study

In this section, we would like to examine how the behavior of the similarity waves varies with several controlling parameters, including the index n in the power–law permeability relation (2.1), the prescribed melting rate Γ, and the density ratio ρ_r. For mathematical simplicity, all the studies in this section are conducted in the linear case only.

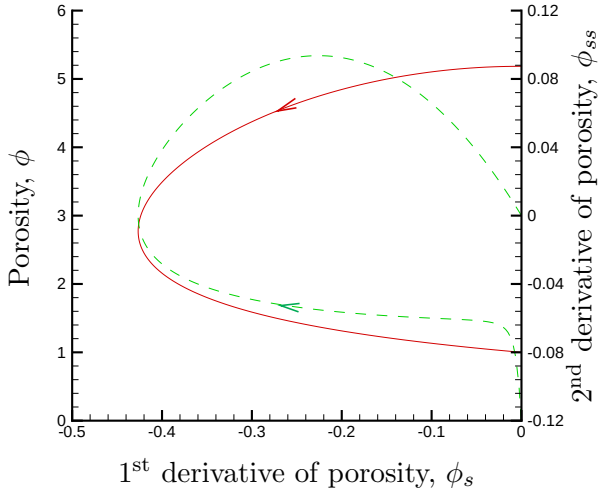

Figure 7: Phase diagram for the similarity wave in the cylindrical case ($c = 10$). Here the solid line presents ϕ versus ϕ_s, while the dashed line presents ϕ_{ss} versus ϕ_s.

6.1 Effect of the K–ϕ Relation

The variation of the permeability K with the porosity ϕ has been widely investigated since it governs the flow in porous media. According to McKenzie [3], a commonly accepted relationship between K and ϕ is the Blake–Kozeny–Carman equation

$$K = \frac{r^2 \phi^3}{w\,(1-\phi)^2}\,, \tag{6.1}$$

where r is the radius of the grains, and w is a constant factor chosen to fit the experimental data. For example, to fit those data measured by Maaløe & Printzlau [9], $w = 1000$ needs to be used [3]. In the case of small degree of melting ($\phi \ll 1$), the least–square power–law best–fit for eq. (6.1) subjected to $0 \le \phi \le 0.15$ yields $K \propto \phi^{3.0987}$. This result leads subsequent investigators to use $n = 3$ for eq. (2.1).

Here, however, we would like to investigate the effect of a positive value of n other than 3 on the behavior of the linear similarity waves for the melting–free case, particularly on the maximum value of the porosity solution. Following the same approach that we employed earlier in section 4.3, one can prove that Theorem 2 holds for all positive values of n. For any given positive value of n, it follows that the first integral of eq. (4.9) becomes:

$$c\lambda\phi^n\phi_{ss} = c(\phi - 1) + (1 - \phi^n)\,, \tag{6.2}$$

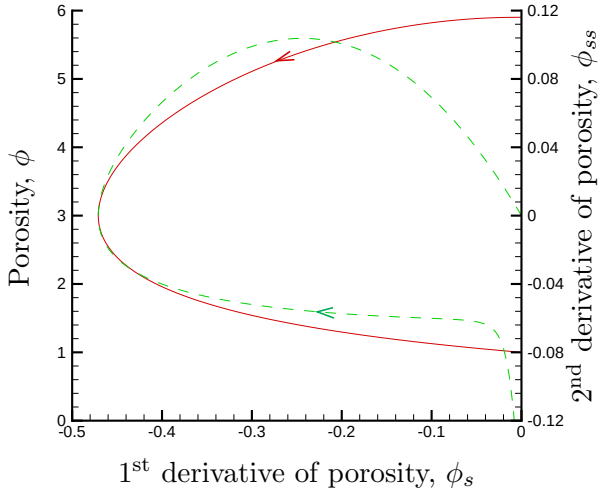

Figure 8: Phase diagram for the similarity wave in the spherical case ($c = 10$). Here the solid line presents ϕ versus ϕ_s, while the dashed line presents ϕ_{ss} versus ϕ_s.

where $c > n$. This will be used as the starting point for our study.

Case 1: $n = 0$ **(constant permeability)**

When $n = 0$, eq. (6.2) becomes

$$\lambda \phi_{ss} = \phi - 1 \,. \tag{6.3}$$

Together with eq. (4.6), this leads to

$$\lambda \phi_s^2 = (\phi - 1)^2 \,. \tag{6.4}$$

Equation (6.4) shows that $\phi_s = 0$ can only when $\phi = 1$. This implies that with the inner boundary condition (4.7) the porosity reaches 1 at the inner boundary. Therefore, one can conclude, based on Theorem 2, that only the trivial solution can exist in this case.

Case 2: $n = 1$

For this case, eq. (6.2) becomes

$$c\lambda \phi \phi_{ss} = (c - 1)(\phi - 1) \,, \tag{6.5}$$

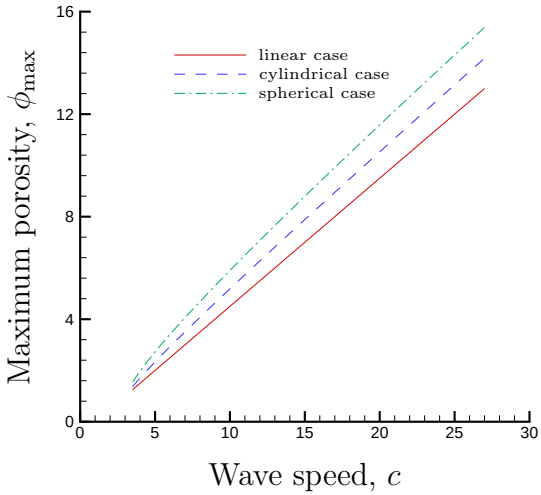

Figure 9: The maximum porosity of the solution versus the wave speed

and there exists a second integral as follows:

$$c\lambda\phi_s^2 = 2(c-1)(\phi - \ln\phi - 1)\,. \tag{6.6}$$

Since $c > n = 1$, here we see that $\phi - \ln\phi - 1 = 0$ wherever $\phi_s = 0$. It can be easily proved that $\phi - \ln\phi - 1$ increases with ϕ when $\phi > 1$, and it decreases with ϕ when $0 < \phi < 1$. Meanwhile, $\phi - \ln\phi - 1 = 0$ when $\phi = 1$. Therefore, $\phi = 1$ is the only root of $\phi - \ln\phi - 1 = 0$ for $\phi > 0$. This implies that $\phi = 1$ at the inner boundary. Once again, because of Theorem 2, only the trivial solution can exist in this case.

Case 3: $n = 2$

For this case, eq. (6.2) becomes

$$c\lambda\phi^2\phi_{ss} = (\phi - 1)(c - \phi - 1)\,, \tag{6.7}$$

which, along with eq. (4.6), leads to a second integral as follows:

$$\frac{1}{2}c\lambda\phi_s^2 = c\left(\ln\phi + \frac{1}{\phi} - 1\right) + \left(2 - \phi - \frac{1}{\phi}\right)\,. \tag{6.8}$$

It can be observed that the following theorem holds in this case.

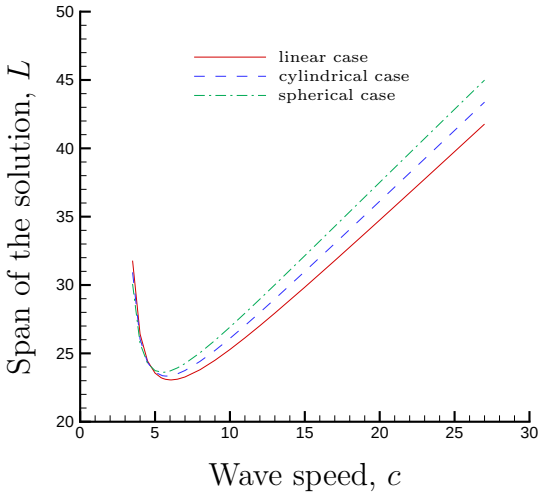

Figure 10: The span of the solution versus the wave speed

Theorem 11. *The non–trivial solution for $n = 2$ satisfies $\phi > 1$ everywhere, and the maximum of the solution, which occurs at $s = 0$ only, is greater than $c - 1$. Furthermore, the solution is monotonically decreasing everywhere.*

Proof. For simplicity of notation, we define a function F of ϕ such that

$$F(\phi) = c\left(\ln\phi + \frac{1}{\phi} - 1\right) + \left(2 - \phi - \frac{1}{\phi}\right) .$$

It is easy to see that the derivative of $F(\phi)$ with respect to ϕ satisfies

$$F'(\phi) = -\frac{\phi - 1}{\phi^2}\left(\phi - c + 1\right) .$$

Since $F'(\phi) < 0$ for $0 < \phi < 1$, $F(\phi)$ decreases with ϕ when $0 < \phi < 1$. Similarly, one can see that $F(\phi)$ increases with ϕ when $1 < \phi < c - 1$, and it decreases with ϕ when $\phi > c - 1$. Since $F(1) = 0$ and $F(\infty) < 0$, $F(\phi) = 0$ has only two roots: one is $\phi = 1$, and the other is some $\phi_* > c-1$. Since in a non–trivial solution $\phi \neq 1$ everywhere (Theorem 2), $\phi = \phi_* > c - 1$ wherever $\phi_s = 0$, including at the inner boundary. Furthermore, according to eq. (6.7), $\phi_{ss} < 0$ when $\phi > c - 1 > 1$. Therefore the extrema of the solution are all maxima. In other words, the solution has no minimum point.

Now that $s = 0$ is a maximum point for the solution, it is impossible for the solution to have any maximum point in $s \in (0, \infty)$, because that requires the existence of at least

one local minimum point where $\phi < \phi_*$, which is already proved impossible. In fact, for the same reason, one can further conclude that the solution is monotonically decreasing with $s \in [0, \infty]$. Now, given that $\phi = c - 1 > 1$ at the inner boundary, $\phi \to 1$ at the outer boundary, and the solution is monotonically decreasing in between, one could claim that $\phi > 1$ everywhere. □

We actually solved the equation $F(\phi_*) = 0$ to determine the variation of the maximum of the solution ϕ_* with the wave speed c. The results are plotted in Figure 11, where the solid line presents the computed value of ϕ_*, the dash-dot line presents a power-law fit $\phi_* = 1.01(c-1)^{1.4}$, and the dashed line presents the lower bound $c - 1$ of ϕ_*, which is revealed by Theorem 11. As we can see here, the power–law fit provides a pretty good estimate of ϕ_* for c up to about 40.

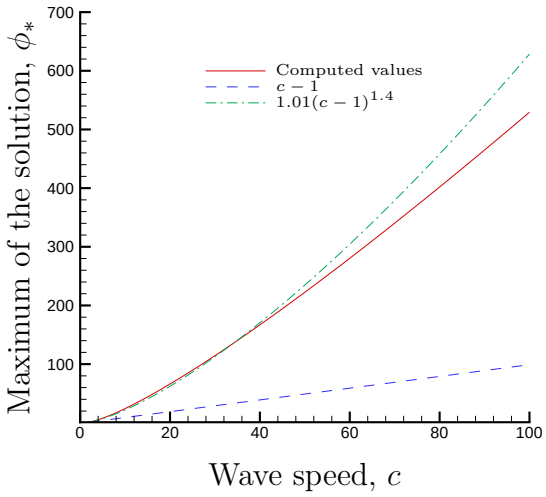

Figure 11: The maximum of the solution versus the wave speed in the linear case ($n = 2$)

Case 4: Other positive value of n

Dividing every term of eq. (6.2) by ϕ^n, multiplying by ϕ_s and then integrating, the following equation is obtained:

$$\frac{1}{2} c\lambda \phi_s^2 = \frac{c}{2-n}\left(\phi^{2-n} - 1\right) - \frac{c-1}{1-n}\left(\phi^{1-n} - 1\right) - (\phi - 1)\,. \tag{6.9}$$

Based on this equation, we can further prove the following theorem.

Theorem 12. *The non–trivial similarity solution only exists for $n>1$. It is larger than 1 everywhere, and it is a monotonically decreasing function of s. The maximum value of the porosity ϕ^* occurs at $s=0$ and it satisfies $\phi^n-1\geq c(\phi-1)$.*

Proof. First of all, the non–trivial solution is greater than 1 everywhere. Otherwise it has to reach 1 at least once, which contradicts Theorem 2.

Next, let us define a function F_n of ϕ such that

$$F_n(\phi)=\frac{c}{2-n}\left(\phi^{2-n}-1\right)-\frac{c-1}{1-n}\left(\phi^{1-n}-1\right)-(\phi-1)\,.$$

The derivative of F_n with respect to s satisfies

$$F_n'(\phi)=\phi^{-n}\left[c(\phi-1)-(\phi^n-1)\right]\,.$$

For $0<n<1$, it is easy to see that $c(\phi-1)-(\phi^n-1)$ increases with ϕ when $\phi>1$, given that $c\geq n$. Thus $F_n(\phi)$ monotonically increases with ϕ when $\phi\geq 1$. Since $F_n(1)=0$, we see that there is no root greater than 1 for $F_n(\phi)=0$, or equivalently, for $\phi_s=0$. Therefore, the solution must reach 1 at the inner boundary, which yields the trivial solution.

For $n>1$ and $n\neq 2$, on the other hand, ϕ^n-1 increases more rapidly than $\phi-1$ when $\phi>1$. Since $F_n(\phi\to 1^+)\sim(c-n)(\phi-1)>0$, and $F_n(\infty)\to-\infty$, there is only one root ϕ_1 of $F_n'(\phi)=0$ for $\phi>1$. When $1<\phi<\phi_1$, $F_n'(\phi)$ is positive, and so is $F_n(\phi)$. For $\phi>\phi_1$, $F_n'(\phi)$ is always negative, which means that $F_n(\phi)$ monotonically decreases with ϕ. Since $F_n(1)=0$, and $F_n(\phi)\to-\infty$ as $\phi\to\infty$, one can conclude that $F_n(\phi)=0$ has one and only one root ϕ_* in the interval (ϕ_1,∞). Furthermore, since $c(\phi-1)-(\phi^n-1)<0$ when $\phi>\phi_1$, it can be observed from eq. (6.2) that $\phi_{ss}<0$ when $\phi=\phi_*$, which means ϕ_* is the maximum of the solution. Therefore, the solution has no minimum point. Following the same approach as what we did earlier for $n=2$ case, we can claim that the solution is monotonically decreasing everywhere. □

A practical value of n is 3, which leads to a neat form of ϕ_* as $\phi_*=\dfrac{c-1}{2}$. For any other values of $n>1$, one can determine the correspondence between ϕ_* and the wave speed c using dichotomy. Results for several values of n are shown in Figure 12. It shows that ϕ_* increases, not necessarily linearly though, with c, but the increase rate decreases as c increases. Particularly, ϕ_* increases much more rapidly with c in the case $1<n<2$ than in the case $n\geq 2$. On the other hand, for the same value of c, ϕ_* decreases with n.

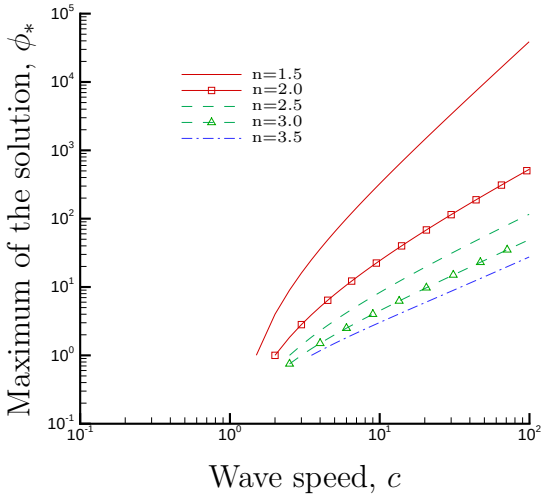

Figure 12: The maximum of the solution versus the wave speed in the linear case ($n>1$)

6.2 Effect of Passive Melting Γ

The melting rate Γ describes mass exchange between the two phases per unit volume per unit time. While the wave propagation regulates the overall profile of the porosity, a non–zero melting rate, which serves as the source term in eq. (3.1), affects mostly the local value of porosity. With the melting rate $\Gamma \neq 0$, eq. (3.1) no longer possesses the close form of the first and second integrals, and thus all theorems found in subsection 4.3 may not be valid anymore. This means that there could be dramatic changes in the behavior of the solution caused by the presence of melting.

For simplicity, we assume that the effect of melting is very much confined so that the melting rate is non–zero only in a relatively narrow region. Physically this assumption means that the melting effect is just a minor factor affecting the flow, compared with the buoyancy effect which governs the flow. Mathematically it means the outer boundary conditions (4.6) can be kept intact. In this study, we choose the following form of melting rate:

$$\Gamma(s) = \Gamma_0 \exp\left(-\frac{s}{l}\right) , \tag{6.10}$$

where Γ_0 is the magnitude of the melting rate profile, and l is the length scale of that profile, which describes how rapidly the melting rate decays. According to eq. (5.4), in the absence of melting effect, the solution decays as $\exp\left(-\sqrt{\dfrac{c-3}{c\lambda}}\, s\right)$ in the far field.

For this far field behavior to be the same with the presence of melting effect, at least the melting rate has to decay more rapidly than the far field solution, i.e.,

$$l < \sqrt{\frac{c}{c-3}} \tag{6.11}$$

Now, for a linear definition of the similarity variable $s = ax + by + \zeta$ and $n = 3$, eq. (4.4) becomes

$$\begin{aligned} &c\phi_s + \Gamma_0(\rho_r - 1)\exp\left(-\frac{s}{l}\right) - c\lambda\phi^3\phi_{sss} - 3c\lambda\phi^2\phi_s\phi_{ss} - 3\phi^2\phi_s \\ &\quad + \frac{3}{l}\lambda\Gamma_0\left(1 - \frac{1}{\rho_r}\right)\exp\left(-\frac{s}{l}\right)\phi^2\phi_s - \frac{1}{l^2}\lambda\Gamma_0\left(1 - \frac{1}{\rho_r}\right)\exp\left(-\frac{s}{l}\right)\phi^3 = 0\,, \end{aligned} \tag{6.12}$$

where $\lambda = a^2 + b^2 + 1$. It can be observed that there's no close form of the first integral, thus we have to solve the original 3^{rd}–order system. To do that, we apply the same approach as what we did earlier for the quadratic cases without melting effect. Computation has been performed for $c = 10$, $\Gamma_0 = 0, \pm 5, \pm 10$, and $l = 0.2, 1.0$. The value of the density ratio ρ_r has been chosen as 1.18 based on the values listed in Table 1. Results corresponding to $l = 0.2$ are shown in Figure 13. For this specific case, while the shape of the solution is qualitatively very similar to what's in the melting–free case, the features of the solution, such as the maximum and the span, are quantitatively different. Figure 13 shows that solutions with $\Gamma > 0$ are greater than those with $\Gamma < 0$ case almost everywhere, except in the neighborhood of the inner boundary. Correspondingly, the span of the solution monotonically increases with Γ. In fact, this is not a surprise, because in case that $\Gamma > 0$ the porosity wave can get reinforced from the melting during its propagation, and thus it is capable of affecting a larger domain. On the other hand, if $\Gamma < 0$, then the porosity wave gets attenuated by losing some melt to solidification process, and thus the wave will be more confined, as far as its span is concerned. The situation for the maximum of the solution, however, is a little bit different. It can be observed that as Γ_0 increases the maximum of the solution generally increases, except for large positive value of Γ_0. In fact, when $\Gamma_0 = 10$, the solution increases with s at the neighborhood of $s = 0$, which is something never occurs in the absence of the melting rate. We suspect this is because in the neighborhood of $s = 0$ the melting effect is so strong that it's no longer a minor factor for the local flow.

For comparison, we also carried out computations for $l = 1.0$. Results from this case are plotted and compared with the results from $l = 0.2$ case in Figure 14. It shows that when $\Gamma < 0$, the maximum of the solution decreases, and the solution becomes smaller everywhere as l increases. When $\Gamma > 0$, the maximum of the solution increases, and

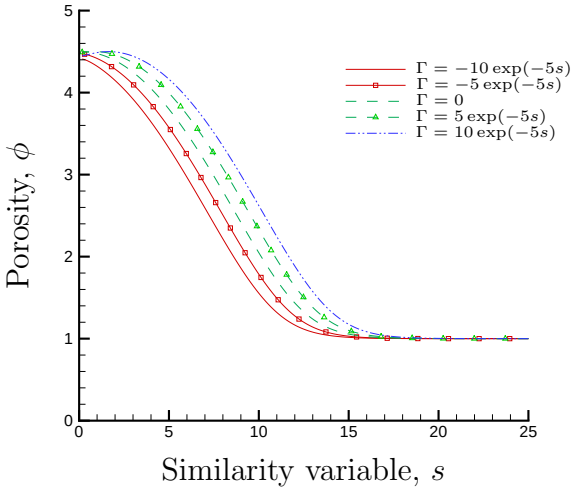

Figure 13: Solutions corresponding to melting rate profile with $l = 0.2$ in the linear case ($n = 3$, $c = 10$, $\rho_r = 1.18$)

the solution becomes greater everywhere as l increases. All these are consistent with the intuitive thinking that the effect of melting becomes more important as l increases. The span of the solution, on the other hand, seems not affected by the value of l.

6.3 Effect of Density Ratio ρ_r

Equation (4.4) clearly shows that the density ratio ρ_r plays a role only when the melting rate Γ is not zero. Once again, the exponentially decaying melting rate (6.10) is employed. Several values of ρ_r that exceed 1, including $\rho_r = 1.18, 1.5, 2.0, 3.0$, and 4.0, are used for studying the effect of the density ratio on the behavior of the similarity solution in the linear case. Results of this study are plotted in Figure 15, which shows that the shape of the solution undergoes significant changes as ρ_r varies. One of those changes is that, while the maximum porosity doesn't change as ρ_r varies, the location of the maximum does change. In fact, it shifts from the inner boundary to somewhere in the domain. For small values of ρ_r, as ρ_r increases, the maximum point moves further away from the inner boundary. At the same time, the porosity value at the inner boundary decreases, and the span of the solution increases. However, this trend reverses after ρ_r passes a certain number between 2.0 and 3.0.

In fact, one can see, from eq. (6.12), that the effect of the density ratio is mostly

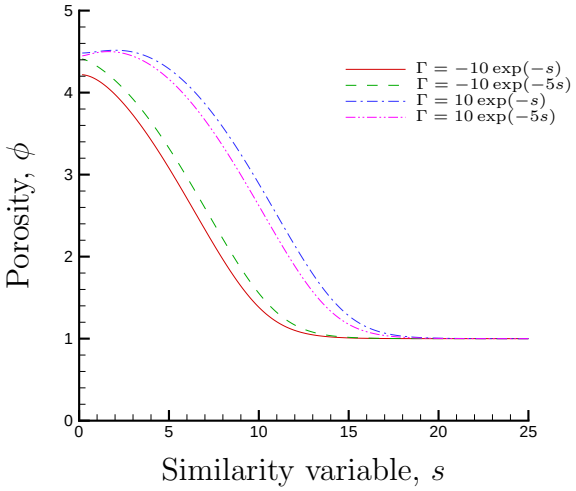

Figure 14: Profiles of the solutions versus the length scale of the melting rate profile in the linear case ($n = 3$, $c = 10$, $\rho_r = 1.18$)

combined with the effect of the melting rate in the $(\rho_r - 1)\Gamma$ term, especially when we consider a melting rate profile with a small length scale l. Therefore, what is shown in Figure 15 can be interpreted as the resultant sequences of increasing the magnitude of the melting. As we can see here, to maintain the inner boundary condition, the system has two ways to adjust the wave propagation. One way is to increase the wave span, which is what happens when ρ_r is small. However, somehow there seems to be a upper limit of the wave span for each value of the wave speed. After the wave span reaches that value, the system can only increase the porosity value at the inner boundary to adjust the wave propagation. When the porosity value at the inner boundary increases to the same level as the maximum of the solution, there will be no way for the system to maintain the "$\phi_s = 0$" condition at the inner boundary. In that case, the melting effect becomes at least a comparable factor as the buoyancy effect, if not the dominant one for the flow, and our mathematical model will break down under these conditions.

7 Concluding Remarks

Compaction is an important process for the segregation and migration of molten rocks. Using a two–phase fluid approach, in which both the solid matrix and the melt are

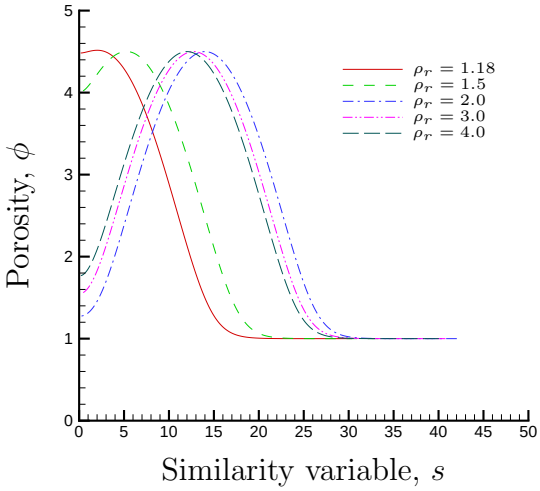

Figure 15: Profiles of the solution versus the density ratio in the linear case ($n = 3$, $c = 10$, $\Gamma_0 = 10.0$, $l = 1.0$)

treated as fluids, one can set up the governing equations for the compaction system and then determine the evolution of the system using numerical methods.

Because of the viscous deformability and permeability of the solid matrix, waves are likely to form and propagate at some stage during the compacting process. Determining wave solution actually becomes an important part of the compaction study. With great mathematical convenience, similarity waves in the systems with low ambient porosity have drawn a lot of attention and are discussed in detail in this paper. Particularly, in the absence of the melting effect, the following conclusion can be arrived through this study:

i) The similarity solution is a monotonically decreasing function of the similarity variable, and the only maximum point is at the inner boundary.

ii) The similarity solution becomes greater everywhere as the dimension of the solution increases, indicating that the system has a greater capacity of transporting the information of the porosity disturbances.

iii) The power index in the permeability relationship controls the existence of the non–trivial solution. For the cases we studied, the non–trivial solution exists only when both K and $\dfrac{\mathrm{d}K}{\mathrm{d}\phi}$ are increasing function of ϕ. This is consistent with Spiegelman's study[5].

With the presence of the melting effect, it has been found that both the melting rate and the density ratio play important roles in determining the behavior of the solution. Totally different features occur when the melting effect become comparable to the buoyancy effect.

It should be noted that similarity solutions only exist in an intermediate stage of the evolution of the system. They are not valid in the initial transition stage, and they may not sustain. To understand how those waves are formed in response to a given porosity disturbance, one needs to solve the governing PDEs (2.7)—(2.10) to determine the details of the transition process. To determine whether and how the similarity wave evolves into another state, one needs to either carry out stability analysis for the similarity waves or use the similarity solution as the initial condition to solve the governing PDEs.

So far most of the compaction study are carried out for the case of small ambient porosity, where a power law for the permeability K and constant viscosities ξ, η for the solid matrix are both reasonable assumptions. When the ambient porosity is not small, both of them need to be modified. Rabinowicz *et al.*[10] did some numerical studies for the melt–free case with porosity up to 40% based on a circulation–percolation interpretation of the two–fluid model. Their results suggested that magma chambers with a kilometer extent are likely resulted from the compaction of a mantle mush with an initial porosity exceeding 5%.

Finally, to fully understand the behavior of the compaction system, both the dynamics and the thermal aspects need to be considered. In that case melting, the phase change between the solid matrix and melt, is no longer passive since it actually depends strongly on the pressure and temperature. The resultant set of the governing equations is thus a strongly coupled system. Before that system can be treated computationally in the future, a number of further studies of the simplified systems need to be carried out for a better understanding of the compaction process.

Acknowledgment

The authors would like to thank Cambridge University Press for granting permission to reprint Figure 1.

References

[1] Barcilon V. and Richter F. M. Nonlinear waves in compacting media. *J. Fluid Mech.*, 164:429–448, 1986.

[2] Scott D. and Stevenson D. J. Magma ascent by porous flow. *J. Geophys. Res.*, 91(B9):9283–9296, 1986.

[3] McKenzie D. P. The generation and compaction of partially molten rock. *J. Petrol.*, 25:713–765, 1984.

[4] Richter F. M. and McKenzie D. P. Dynamical models for melt segregation from a deformable matrix. *J. Geology*, 92:729–740, 1984.

[5] Spiegelman M. Flow in deformable porous media. part 1: Simple analysis. *J. Fluid Mech.*, 247:17–38, 1993.

[6] Barcilon V. and Lovera O. M. Solitary waves in magma dynamics. *J. Fluid Mech.*, 204:121–133, 1989.

[7] Spiegelman M. Physics of melt extraction: Theory, implications and applications. *Trans. Roy. Soc. London*, 342:23–41, 1993.

[8] Wiggins C. and Spiegelman M. Magma migration and magmatic solitary waves in 3-D. *Geophys. Res. Let.*, 22(10):1289–1292, 1995.

[9] Maaløe S. and Printzlau I. Natural partial melting of spinel lherzolites. *J. Petrol.*, 20:727–741, 1979.

[10] Rabinowicz M., Genthon P., Ceuleneer G., and Hillairet M. Compaction in a mantle mush with high melt concentrations and the of magma chamber. *Earth and Planetary Sci. Let.*, 188:313–328, 2001.